ON-LINE APPENDIX

MR Imaging Acquisition

All MR images were acquired in axial sections with a 1.5T or 3T scanner. We acquired the following imaging sequences and parameters: T1-weighted postcontrast images were a spin-echo sequence with the following range of parameters—section thickness = 3.0–5.0 mm, TR = 400–750 ms, TE = 2.45–17 ms, flip angle = 90°. FLAIR images were acquired with inversion recovery turbo spin-echo with the following ranges of parameters: section thickness = 3.0–5.0 mm, TE = 109–129 ms, TR = 9000 ms, flip angle = 150°. Similarly, T2-weighted MR images were acquired with turbo spin-echo: section thickness = 3.0–5.0 mm, TE = 100 ms, TR = 4000 ms, flip angle = 150°.

Preprocessing of MR Imaging Sequences

For every patient study, all the available MR imaging protocols (T1WI, T2WI, FLAIR) were coregistered with reference to T1-weighted MR imaging by using 3D affine registration with a 12-*df* encoding rotation, translation, sheer, and scale via 3D Slicer. To account for resolution variability, during registration, we resampled every MR imaging section to a uniform pixel spacing of 0.5×0.5 mm^2 and we interpolated every MR imaging volume to 3-mm section thickness. We then corrected every study for intensity nonstandardness. "Intensity nonstandardness" refers to the inherent signal intensity drift between different MR imaging acquisitions due to which image intensities do not have a fixed tissue-specific numeric meaning, even within the same protocol for the same body region or for images of the same patient obtained on the same scanner.[1] Correction for intensity nonstandardness was implemented by using the approach described by Madabhushi and Udupa[1] and implemented in Matlab R2014b (MathWorks) (On-line Fig 2). Additional preprocessing involved skull stripping and bias field correction. Skull stripping was performed via an open-source automated BrainSuite tool (http://brainsuite.org), while bias field artifacts were corrected for with the popular N3 algorithm.[2]

Description of Texture Features

Haralick Texture Features. Haralick features are based on quantifying the spatial gray-level co-occurrence within local neighborhoods around each pixel in an image, stored in the form of matrices. Thirteen Haralick texture descriptors were calculated from every lesion for every sequence by computing the median of the statistics derived from the corresponding co-occurrence matrices.

Laws Texture Features. Laws features use 5×5 separable masks that are symmetric or antisymmetric to extract level, edge, spot, wave, and ripple patterns on an image.[3] The convolution of these masks with every image resulted in 25 distinct Laws features for each image for every MR imaging sequence.

Laplacian Pyramids. Laplacian pyramids allow capturing multiscale edge representations via a set of bandpass filters.[4,5] First, the original image is convolved with a Gaussian kernel. The Laplacian is then computed as the difference between the original image and the low-pass-filtered image. The resulting image is then subsampled by a factor of 2, and the filter subsample operation is repeated recursively. This process is continued to obtain a set of bandpass-filtered images (because each is the difference between 2 levels of the Gaussian pyramid). Twenty-four filtered image representations are obtained from every lesion for every MR imaging sequence by computing the median of feature values across all pixels within a lesion.

Histogram of Gradient Orientations. For every pixel c on an image, gradients along the X and Y direction are computed as ∂X and ∂Y.[5,6] The gradient orientation is then computed as $\theta(c) = \tan^{-1}(\partial Y/\partial X)$. After one obtains the gradient orientation at every pixel, within the segmented lesion, the pixels are binned into a histogram, spanning 0°–360°. The entire histogram is binned in 20 bins, with each bin spanning 18°. The feature vector consists of binned histogram values in the form of vectors of 20×1 in length.

REFERENCES

1. Madabhushi A, Udupa JK. **New methods of MR image intensity standardization via generalized scale.** *Med Phys* 2006;33:3426–34 CrossRef Medline
2. Sled JG, Zijdenbos AP, Evans AC. **A nonparametric method for automatic correction of intensity nonuniformity in MRI data.** *IEEE Trans Med Imaging* 1998;17:87–97 Medline
3. Laws K. *Textured Image Segmentation* [dissertation]. Los Angeles: University of Southern California; 1980
4. Burt PJ, Adelson EH. **The Laplacian pyramid as a compact image code.** *IEEE Trans Commun* 1983;31:532–40
5. Prasanna P, Dana KJ, Gucunski N, et al. **Automated crack detection on concrete bridges.** *IEEE Trans Automation Sci Eng* 2016;13:591–99 CrossRef
6. Dalal N, Triggs B. **Histograms of oriented gradients for human detection.** *IEEE Comput Soc Conf Comput Vis Pattern Recognit* 2005;1:886–93

On-line Table 1: Category of texture features evaluated in this work and the possible explanation of the biologic underpinning associated with RN or tumor recurrence in brain tumors

Feature Category	Descriptor	Intuitive Description	Relevance to Tumor/Radiation Necrosis Organization
Haralick features (repeated occurrence of gray-level configuration in the texture represented by the GLCM	IDM	IDM is a reflection of the presence or absence of uniformity, and hence is a measure of local regions of homogeneity	Captures underlying heterogeneity within the lesion, which may be higher in case of tumor recurrence compared with RN
	Correlation	Quantifies the linear patterns in an image on the basis of the distance parameter	Increased presence of linear patterns yield higher correlation values; lack of image linearity yields lower correlation values
	Sum entropy	Measure of GLCM relationship to distribution of intensity with respect to entropy; entropy is the measure of disorder	Higher entropy is indicative of more chaotic arrangement across tumor recurrence compared with RN
	Sum variance	Measure of GLCM relationship to distribution of intensity with respect to variance	Possibly accounting for greater variation of scattered atypia and local accumulation of mitotic processes as observed on histopathology
Laws features	E5, L5, S5, R5 (combination in both *X* and *Y* directions)	E (Edge) L (Level) S (Spot) R (Ripple)	Possibly accounting for the appearance of ROI described as spreading wave front, soap bubble, or Swiss cheese effect on RN
Histogram of gradient orientations	Per-pixel intensity orientations	Intensity orientation captures prominent direction of intensity change in *X* and *Y* direction for every pixel	Possibly accounting for high cellular activity in recurrence compared with RN
Laplacian pyramids		Multiresolution filters capture edges at different levels	Prominent edges between RN and recurrence not discernible on the original scale

Note:—IDM indicates Inverse Difference Moment; GLCM, gray-level co-occurrence matrix; E, edge; L, level; S, spot.

On-line Table 2: Top 5 features identified on the training cohort by mRmR feature-selection scheme across T1WI, T2WI, and FLAIR sequences on primary and metastatic brain tumor subgroups

Sequence and Primary Brain Tumor Subset: Energy	Metastatic Brain Tumor Subset: Correlation
Gd-T1WI	
Gabor, $\Theta = 22.5$, $\Lambda = 4$	Information measure of correlation
Laws, E5L5	Difference variance (Laplace)
Information measure of correlation	Laws, S5E5
Inertia	Gabor, $\Theta = 45$, $\Lambda = 2$
T2WI	
Correlation (Laplace)	Correlation (Laplace)
Laws, L5E5	Difference variance
Laws, L5E5 (Laplace)	Laws, R5R5
Information measure of correlation	Laws, L5E5
Laws, E5E5	Laws, R5R5 (Laplace)
FLAIR	
Laws, L5E5 (Laplace)	Sum average (Laplace)
Information measure of correlation	Information measure of correlation
Laws, E5E5	Laws, L5S5
Correlation (Laplace)	Haralick, difference variance
Energy (Laplace)	Correlation

On-line Table 3: Ground truth as established from pathologic findings, classifier results, and independent assessment of 2 expert neuroradiologists on 15 studies (11 primary and 4 metastatic) in the holdout set[a]

Subgroup and Study No.	Pathologist Confirmation	Radiomics Consensus	Radiologist 1/Confidence Score (Range, 0.5–1)	Radiologist 2/Confidence Score (Range, 0.5–1)
Primary brain tumor studies				
1	Recurrence	Recurrence	RN (0.6)	RN (0.7)
2	RN	RN	Recurrence (0.6)	Unclear (leaning toward RN) (0.5)
3	Recurrence	Recurrence	RN (0.6)	RN (0.8)
4	RN (30%), recurrent tumor (30%),[b] treated as recurrence	Recurrence	Recurrence (0.6)	Recurrence (0.9)
5	Recurrence	Recurrence	Recurrence (0.7)	Recurrence (1)
6	Recurrence	Recurrence	RN (0.6)	RN (0.6)
7	RN (75%), tumor recurrence (25%),[b] clinically treated as recurrence	Recurrence	RN (0.8)	RN (0.8)
8	Recurrence	Recurrence	RN (0.6)	RN (0.8)
9	Recurrence	Recurrence	RN (0.7)	Recurrence (0.7)
10	Recurrence	RN	Unclear (0.5)	Recurrence (0.6)
11	Recurrence	Recurrence	Recurrence (1)	RN (0.6)
Metastatic brain tumor studies				
1	RN	Recurrence	RN (0.9)	RN (0.7)
2	RN (60%), viable metastatic tumor (40%),[b] clinically treated as tumor recurrence	Recurrence	Recurrence (1)	Unclear (leaning more towards tumor) (0.5)
3	Recurrence	Recurrence	RN (0.8)	RN (0.7)
4	RN (50%) and reactive gliosis, negative for viable neoplastic cells[b]	Recurrence	Unclear (0.5)	Recurrence (0.7)

[a] The confidence scores range between 0.5 and 1 (in increments of 0.1) and denote the confidence that the expert reader had in assigning a case as RN or tumor recurrence. Confidence of 0.5 denotes that the expert was unclear as to the diagnosis based just on the routine MRI scans, while a confidence of 1 denotes that the expert was completely confident in his or her diagnosis for RN or tumor recurrence.

[b] Cases that had mixed characteristics of both RN and tumor recurrence as found in the pathology report.

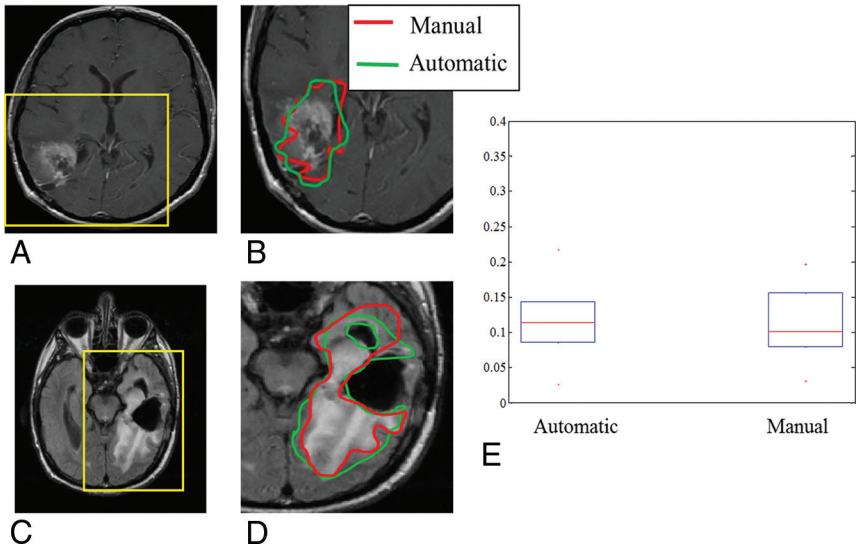

ON-LINE FIG 1. *A* and *C*, Two MR images from 2 different patient studies. The corresponding segmentations are shown in *B* and *D*, where red denotes automated segmentation and green denotes manual segmentation. *E*, Box-and-whisker plots for the top FLAIR feature obtained for automatic and manual segmentation for 5 randomly selected studies from the primary brain tumor recurrence subgroup. The differences in feature values obtained from automatic and manual segmentation were found to be statistically insignificant.

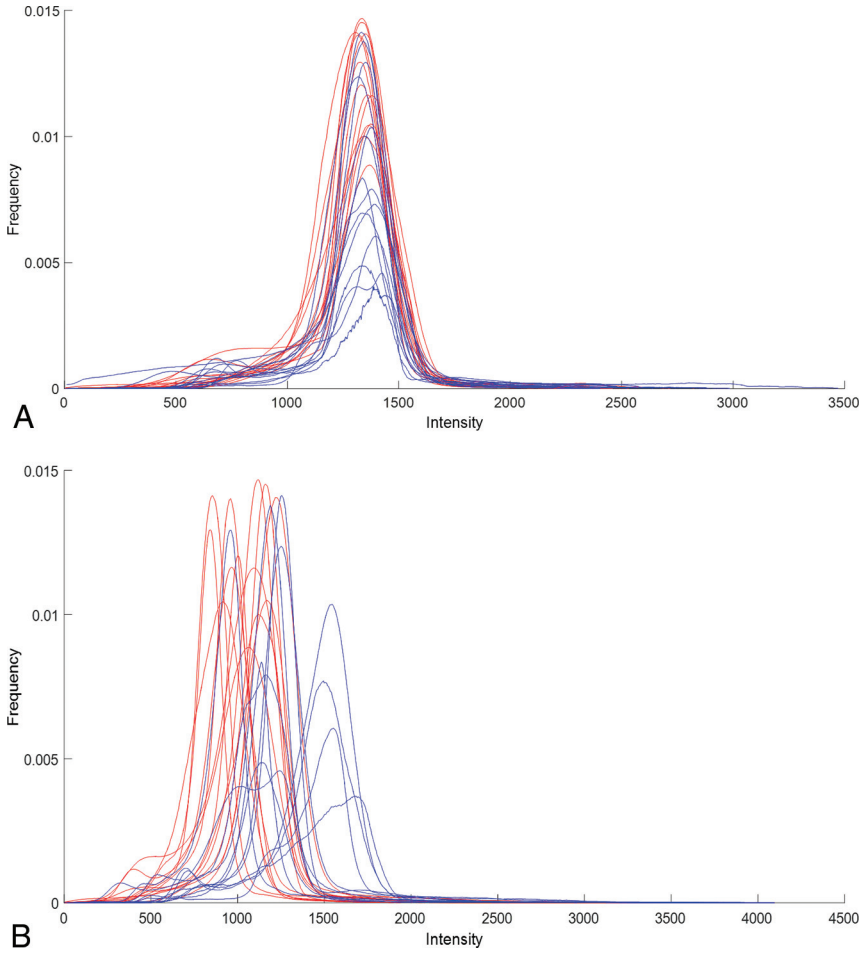

ON-LINE FIG 2. Illustration of intensity drift between the training (red) cohort obtained from the local institution and the holdout (blue) cohort obtained from the collaborating institution for Gd-T1-weighted MR imaging by plotting the distributions of different patient studies along the same axis. Note that after intensity standardization, the distributions across studies from different institutions are no longer misaligned; this outcome suggests successful correction of the drift artifacts.

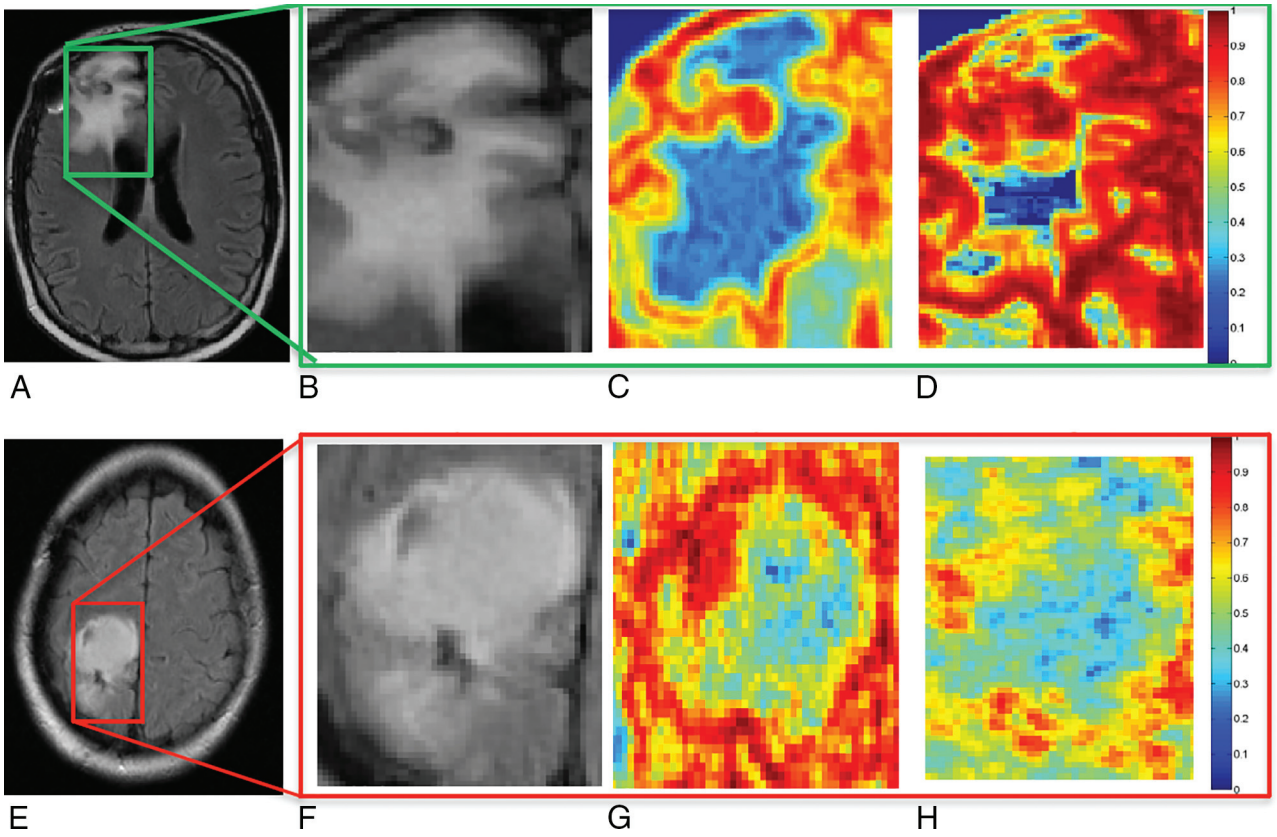

ON-LINE FIG 3. A representative FLAIR section for RN (*A*) and tumor recurrence (*E*) is shown for 2 different metastatic brain tumor studies. *B* and *F* show the original FLAIR images corresponding to RN (*A*) and tumor recurrence (*E*), respectively. *C*, *D*, *G*, and *H*, The top 2 textures corresponding to RN (*A*) and tumor recurrence (*E*), respectively. Red represents a high feature value, while blue represents a low feature value for a given pixel.